Materials Horizons

ROYAL SOCIETY OF CHEMISTRY

COMMUNICATION

View Article Online
View Journal | View Issue

Cite this: *Mater. Horiz.*, 2022, 9, 1641

Received 3rd February 2022,
Accepted 14th April 2022

DOI: 10.1039/d2mh00135g

rsc.li/materials-horizons

Multi-compartment supracapsules made from nano-containers towards programmable release†

Minghan Hu, *[a] Nico Reichholf,[a] Yanming Xia,[bc] Laura Alvarez, ‡[a] Xiaobao Cao, [b] Shenglin Ma,[c] Andrew J. deMello [b] and Lucio Isa *[a]

The assembly of nanomaterials into suprastructures offers the possibility to fabricate larger scale functional materials, whose inner structure strongly influences their functionality for a vast range of applications. In spite of the many current strategies, achieving multi-compartment structures in a targeted and versatile way remains highly challenging. Here, we describe a controllable and straightforward route to create uniform suprastructured materials with a multi-compartmentalized architecture by confining primary nanocapsules into droplets using a cross-junction microfluidic device. Following solvent evaporation from the droplets, the nanocapsules spontaneously assemble into precisely sized multi-compartment particles, which we term supracapsules. Thanks to the process, each spatially separated nanocapsule unit retains its cargo and functionalities within the resulting supracapsules. However, new collective properties emerge, and, particularly, programmable release profiles that are distinct from those of single-compartment capsules. Finally, the suprastructures can be disassembled into single-compartment units by applying ultrasonication, switching their release to a burst-release mode. These findings open up exciting opportunities to fabricate multi-compartment suprastructures incorporating diverse functionalities for materials with emerging properties.

New concepts

In this manuscript, we demonstrate a robust and straightforward method to construct multi-compartment suprastructures from nanocapsules (also known as nano-containers), which we term supracapsules. Beyond the use of conventional nanoparticles as building blocks to make suprastructures, the assembly of nanocapsules opens up an opportunity for introducing multiple compartments within a suprastructure. Compared with the suprastructures made from nanoparticles, supracapsules display the unique ability to incorporate many distinct units that preserve their liquid cargoes and combine their functions. Thanks to the internal multi-compartment structure, supracapsules also display programmable release kinetics that are distinct from single-compartment nanocapsules. Therefore, they provide a flexible and versatile alternative to regulate cargo release, *i.e.* for biomedical applications. We further show that it is possible to disassemble supracapsules on demand through ultra-sonication, adding an external switch for the release of multiple encapsulated cargoes. The understanding of emerging features from multicompartment architectures within supracapsules provides useful insights to design the next generation of suprastructured materials for many advanced applications. We envision that fabricating multi-compartment suprastructures could have significant impact not only in materials science, but also in other research fields such as biomedicine and artificial cells.

Introduction

Suprastructures are 3D objects originated by the assembly of smaller constituents; in particular, they comprise microscale materials constituted by the assembly of colloidal nanoparticles, which are held together as the result of the interplay between their interactions, and that are known as supraparticles.[1–4] One of the most appealing features of assembling suprastructures is the possibility to integrate different nanomaterials to endow the resulting object with multiple functionalities. Often, those assemblies display a collective enhancement of properties compared to the individual nanoscale building blocks and can even show features that are different from those of their constituents.[4–7] In order to direct the properties of the suprastructures, it is therefore not only essential to select and control the properties of nanomaterials that are used as the building blocks for assembly, but also to tailor their inner structure. For instance, by controlling

[a] *Laboratory for Soft Materials and Interfaces, Department of Materials, ETH Zürich, Vladimir-Prelog-Weg 5, 8093 Zürich, Switzerland. E-mail: minghan.hu@mat.ethz.ch, lucio.isa@mat.ethz.ch*
[b] *Institute for Chemical and Bioengineering, Department of Chemistry and Applied Biosciences, ETH Zürich, Vladimir-Prelog-Weg 1, 8093 Zürich, Switzerland*
[c] *Department of Mechanical & Electrical Engineering, Xiamen University, Xiamen, Fujian, China*

† Electronic supplementary information (ESI) available. See DOI: https://doi.org/10.1039/d2mh00135g

‡ Current address: CNRS, Univ. Bordeaux, CRPP, UMR5031, Pessac, France.

colloidal interactions during assembly, the internal architectures of supraparticles can be varied from those of close-packed spheres[8] to the ones of Janus-like,[9–12] core–shell,[13–15] or mesoporous structures.[2,16–18] Thanks to the existence of a vast range of synthetic nanomaterials and assembly strategies, supraparticles have shown outstanding performance in applications including catalysis,[3,19] photonics,[20–22] and microrobotics.[23–25]

In spite of these advances, producing suprastructures with multiple internal compartments remains a significant challenge. Multi-compartmentalized materials have a structure that confines two or more distinct domains loaded with different cargoes, which are simultaneously transported and are spatially separated.[26,27] Recently, examples of multi-compartment liposomes,[28–30] polymersomes,[31–33] microgels,[34,35] and capsosomes,[36–38] have emerged as vehicles for multi-drug delivery,[35,39] as hierarchical microreactors,[40] and as cell mimics.[41,42] However, their realization requires either multiple emulsification steps to produce double emulsion droplets or additional post-chemical reactions to form the compartments.[31,36,43]

Here, we present a straightforward assembly approach to produce supraparticles with a multi-compartment structure based on the organization of nanocapsules, instead of commonly used nanoparticles, into a suprastructure by using droplet-templated assembly. We show that dextran-based nanocapsules with various cargoes can be synthesized and then confined into monodisperse oil droplets within an oil-in-water emulsion generated at a flow-focusing microfluidic geometry. After evaporating the oil, the nanocapsules spontaneously organize into close-packed clusters, which we term supracapsules (Fig. 1a). On the one hand, the process leads to supracapsules that have spatially separated compartments, which preserve the functions and properties of the initial nanocapsules. On the other hand, our supracapsules display distinctive release kinetics compared to single nanocapsules, whereby the release profile can be programmed by controlling the properties of the assemblies. Moreover, the supracapsules can be disassembled on demand through ultra-sonication, adding external control to the release profiles of encapsulated cargoes.

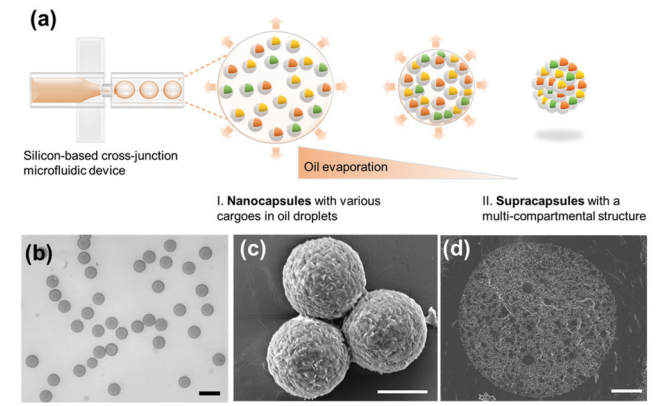

Fig. 1 Fabrication of supracapsules. (a) Assembly scheme of nanocapsules towards the fabrication of supracapsules by evaporation-induced self-assembly from emulsion droplet templates. The spheres of different colors (yellow, red and green) represent nanocapsules with different encapsulated cargoes. (b) Optical micrographs of supracapsules with a monodispersed size, as obtained by microfluidics. (c) SEM image of supracapsules after drying. (d) Cryo-SEM micrograph of the cross-section of a supracapsule after freeze-fracture. Scale bars are 20 μm, 5 μm, and 2 μm in panels (b), (c) and (d), respectively.

Results and discussion

We first synthesized dextran-based nanocapsules with various water-soluble cargoes to act as the building blocks of our supracapsules. Dextran was chosen since it is a biocompatible and biodegradable polymer that has been widely used in biomedical applications.[44,45] Nanocapsules were formed by the polyaddition reaction of dextran at the interface of droplets in a water-in-oil miniemulsion (Fig. S1, ESI†). The resulting dextran-based nanocapsules have an average diameter of 243 ± 92 nm and a 5 nm thick shell (Fig. S3, ESI†), and were dispersed in cyclohexane. Details of the nanocapsule synthesis are provided in the ESI.†

We then proceeded to fabricate the multi-compartment supracapsules by using droplet-templated assembly.[46] In this process, we start from a nanocapsule dispersion in oil (cyclohexane), which is broken into droplets. Upon evaporation of the oil, nanocapsules assembled into spherical clusters. To generate monodisperse cyclohexane droplets, and thus monodisperse supracapsules, we designed and employed a silicon-based microfluidic device containing a cross-junction (Fig. S2, ESI†). Due to the formation of monodisperse droplets at this cross-junction, the resulting supracapsules have a narrow size distribution (Fig. 1b). Closer inspection of the morphology of the supracapsules reveals that they are tightly packed on the surface of the original droplets (Fig. 1c and Fig. S4, ESI†), whilst imaging of the cross-section by means of cryogenic electron microscopy shows that the nanocapsules are packed across the entire supracapsule volume to form a multi-compartment structure (Fig. 1d).

Assuming that the interior structure of the supracapsules is homogeneous (as shown in Fig. 1d), the diameter of the supracapsules (d_{sc}) can be directly predicted based on the droplet size before cyclohexane evaporation (d_{drop}) as follows:

$$d_{sc} = d_{drop} \times \left(\frac{C_{nc}}{f_v}\right)^{\frac{1}{3}} \quad (1)$$

where C_{nc} is the initial volume fraction of nanocapsules in the oil droplets and f_v is the packing density of nanocapsules within the formed supracapsules. According to eqn (1), the size of the supracapsules can be tuned by changing the initial droplet size and the initial concentration of nanocapsules. In a series of experiments, shown in Fig. 2a, we changed the average droplet diameter between 15–30 μm by tuning input flow rates entering the microfluidic device (Table S1, ESI†), and varied the concentration of nanocapsules from 0.9 vol% to 7.1 vol%. Data demonstrate that the diameter of the supracapsules can be precisely tuned between 2 and 20 μm (Fig. 2b), following the predicted scaling; $d_{sc} \propto d_{drop}(C_{nc})^{1/3}$ (Fig. 2c). By

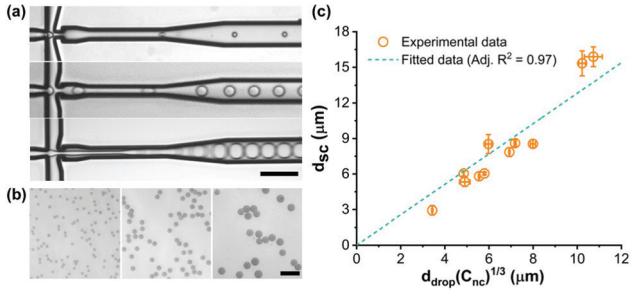

Fig. 2 Tuning the size of supracapsules. (a) Generation of monodisperse oil droplets of various sizes within the microfluidic device, with the droplet size being controlled by the flow rate (scale bar is 50 μm). (b) Images of supracapsules of various sizes (scale bar is 20 μm). (c) Diameter of supracapsules (d_{sc}) as a function of $d_{drop}(C_{nc})^{1/3}$. d_{drop} is the diameter of droplets and C_{nc} is the volume concentration of nanocapsules.

fitting the slope of the data shown in Fig. 2c, we obtain an average packing density of the nanocapsules (f_v) of 0.47 ± 0.07. Based on the value of packing fraction, we estimate that our supracapsules contain from 800 to 130 000 nanocapsules. The high number of compartments may be beneficial for biomedical applications such as therapeutic delivery.[26]

One of the key features of multi-compartmentalized structures is that the separated units should preserve their functions. After establishing accurate size control of supracapsules, we test whether different cargoes are effectively retained after assembly. We therefore produced three different populations of nanocapsules, the first two each encapsulating a different water-soluble fluorescent dye coupled to a high molecular weight polymer (~5000 Da), Cy5-PEG (red) and FITC-PEG (green), respectively, and the third one without any fluorescent dye. We then mixed these three types of nanocapsules in a 1 : 1 : 3 volume ratio in cyclohexane to form supracapsules. After assembly, no appreciable amount of dye is released from the supracapsules over a period of 72 hours (Fig. S6, ESI†). As shown by the high-resolution confocal images in Fig. 3a, the Cy5-PEG and FITC-PEG dyes are localized in separate nanoscale compartments, indicating that our assembly strategy allows the compartmentalization of different payloads. As a further proof that original functions are retained after assembly, we encapsulated superparamagnetic iron oxide nanoparticles (with an average diameter of 10 nm) within the nanocapsules. Fig. 3b shows that the nanocapsules and supracapsules exhibit the same magnetic properties. Moreover, assembly into supracapsules, in which the magnetization of all the constituent nanocapsules is combined, enables easy separation (Fig. 3c and Video S1, ESI†) and manipulation with an external magnetic field (Fig. 3d and Video S2, Fig. S7, ESI†).

Controlled release is an important feature for nanocapsules. After assembly, it is essential to understand how the multi-compartmentalized architecture affects the release profiles from supracapsules. To study their release profiles, Cy5 (M_w = 519 Da without coupled PEG) was used as the model cargo and encapsulated within the nanocapsules. We produced supracapsules with three different average diameters (5 μm, 12 μm and

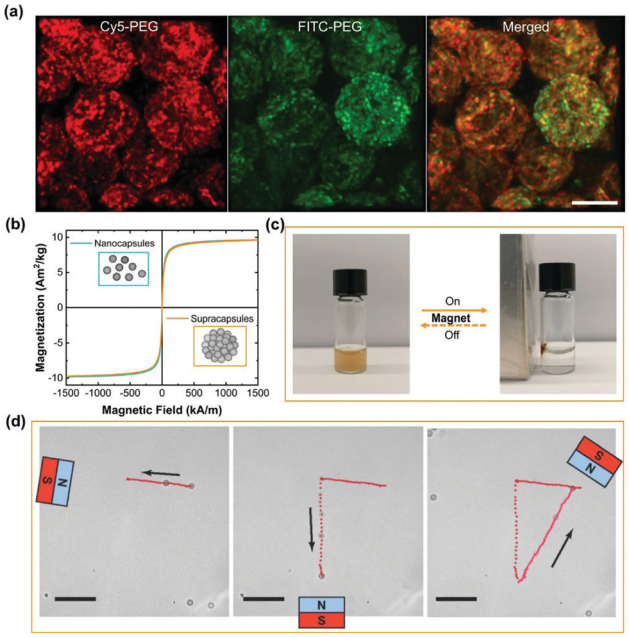

Fig. 3 Multi-functional supracapsules with different cargoes. (a) High-resolution confocal microscopy images of supracapsules assembled using a 1 : 1 : 3 volume ratio of nanocapsules Cy5-PEG (red) : FITC-PEG (green) : non-fluorescent. Scale bar is 5 μm. (b) Magnetic response of nanocapsules encapsulating superparamagnetic nanoparticles and of their assembled supracapsules characterized by vibrating-sample magnetometer. (c) Photographs showing the separation of magnetic supracapsules. (d) Trajectory of a magnetic supracapsule in water under directed magnetic fields. The cartoon insets indicate the positions of the magnet. Scale bars are 50 μm.

16 μm, Fig. 4a) and compared their release profiles with those of individual nanocapsules (having a diameter of 243 ± 92 nm) for the same total Cy5 concentration. As shown in Fig. 4b, the release profiles of Cy5 from both nanocapsules and supracapsules follow an exponential curve, indicating a first-order kinetic process.[47,48] In particular, dye release from the nanocapsules reaches a plateau after 4 hours, while the same amount of nanocapsules assembled into 5 micron supracapsules takes around 6 hours to reach the release plateau. The half-life time of dye release within nanocapsules and supracapsules can be calculated by the exponential curves from Fig. 4b. These values increase as a function of supracapsule diameter, following a quadratic growth model (Fig. 4c). Both the release profiles and the scaling indicate that the release is diffusion-dominated.[48] We can thus assume that the encapsulated Cy5 would diffuse through the polymer shell to a perfect sink with a constant diffusion path length and diffusion coefficient. The hypothesis of a perfect sink is further supported by the fact that the total dye concentration in the system is below the micromolar range and therefore the release rate is not affected by the dye concentration outside of the loaded units (see Methods). The effective release rate (M_t/M_∞) of dyes in nanocapsules and supracapsules can be further calculated based on a model proposed by Crank,[48,49] *i.e.*

$$\frac{M_t}{M_\infty} = \frac{4}{L}\sqrt{\frac{Dt}{\pi}} \quad (2)$$

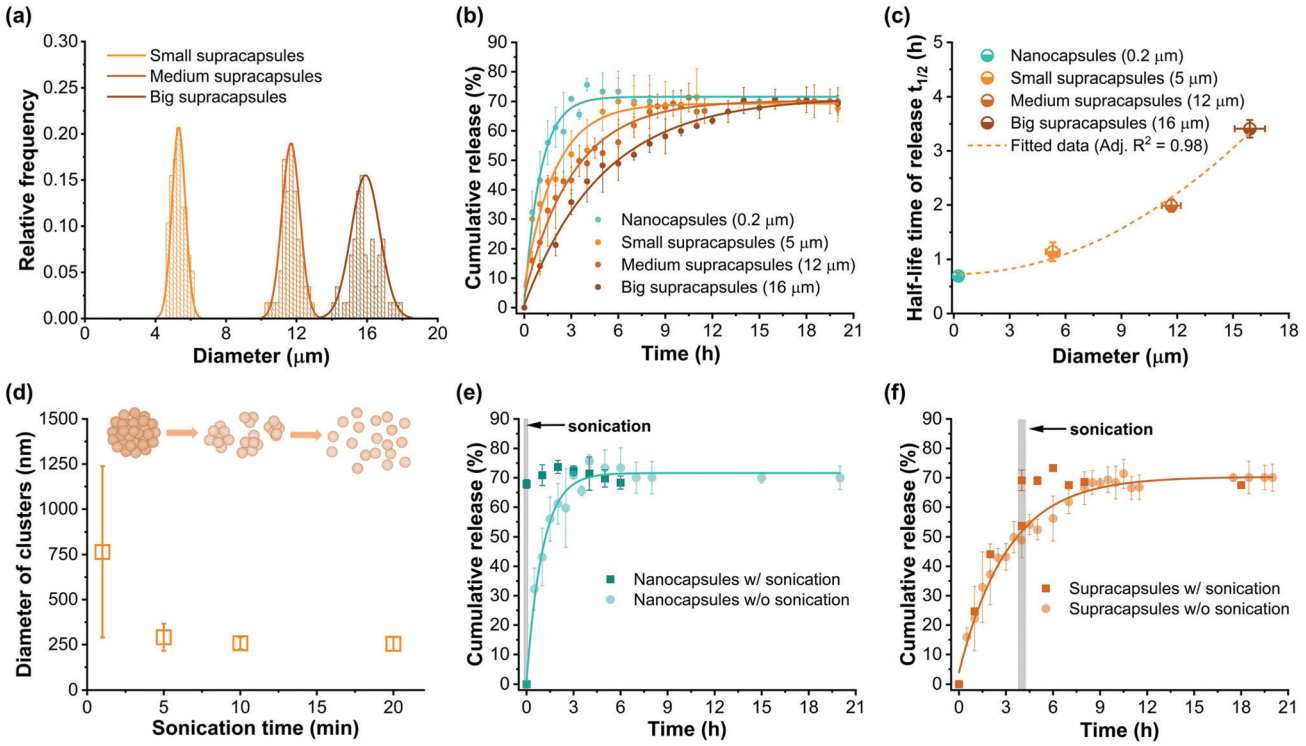

Fig. 4 Programmable release of supracapsules. (a) Size distributions of supracapsules with different average diameters (5 μm, 12 μm and 16 μm, respectively). (b) Release profiles of nanocapsules and supracapsules with various sizes. (c) Half-life time of dye release as a function of the diameter of nanocapsules and supracapsules. (d) Nanocapsule cluster size, ranging from intact supracapsules (12 μm diameter) to individual nanocapsules as a function of sonication time. The inset cartoon schematically shows the disassembly process. (e) Release profiles of nanocapsules without and with sonication. Sonication is applied at the beginning of dye release. (f) Release profiles of supracapsules (with an average diameter of 12 μm) without and with sonication. Sonication is applied when dye has been released for 4 hours.

where M_t and M_∞ are cumulative mass of dye at time t and infinity (plateau), respectively; L is the diffusion path length; D is the effective diffusion coefficient of the dye. In the case of nanocapsules, the shell thickness (5 nm measured by cryo-TEM) is the diffusion path length. Accordingly, the diffusion coefficient of Cy5 in nanocapsules ($D_{\text{nanocapsules}}$) is 4.85×10^{-22} m^2 s^{-1}, and the effective D of Cy5 in supracapsules decreases to 1.02×10^{-22} m^2 s^{-1} (Table S2, ESI†).

Since the assembled nanocapsules are held together by van der Waals forces, they can be physically separated by application of a strong external energy input. Indeed, we show that after sonication for one minute, 12 μm diameter supracapsules disassembled to small clusters with an average diameter of 764 ± 474 nm. After 5 minutes sonication, the size of clusters further decreased to 291 ± 75 nm, indicating that the supracapsules completely disassemble into single nanocapsules (Fig. 4d). Additionally, sonication enables the further tuning of the release profile of encapsulated cargoes. For example, once sonication is initiated, Cy5 is completely released within minutes (Fig. 4e). This phenomenon also agrees with reported burst-release behaviour in other types of nanocapsules.[50,51] Significantly, we were able to take advantage of this feature and use it to tune the release behaviour of supracapsules. As shown in Fig. 4f, supracapsule release kinetics can be changed from a "sustained-release" mode to a "burst-release" mode upon sonication. After sonication, all the dye molecules contained within supracapsules are completely released with the profile reaching the same plateau.

Conclusions

Our results demonstrate that the assembly of nanocapsules into a multi-compartment suprastructure, which we term supracapsules, is possible *via* droplet-templated assembly within a microfluidic device. This assembly approach can easily produce uniform multi-compartment objects thanks to the monodispersed droplets generated by the microfluidic device. The diameter of the supracapsules can then be easily tuned by changing droplet size and nanocapsule concentration during the process. Due to the flexibility of this assembly strategy, we successfully combined different units, *i.e.* nanocapsules with different types of cargoes, into multi-compartment suprastructures while preserving the encapsulated cargoes and their functions. In addition to the model systems studied herein, this flexible strategy can be extended to nanocapsules containing other cargoes, *e.g.* with a series of enzymes for multi-component microreactors as cell mimics.[37,42]

One of the key features of using nanocapsules is that the entrapped cargoes can be controllably released *via* diffusion

through the nanocapsules' shells. Compared with single-compartment nanocapsules, multi-compartment supracapsules present distinctive and programmable release profiles owing to their internal structure, which provide a more flexible and versatile alternative to systems that require additional coatings to regulate cargo release.[52–54] Furthermore, sonication can be used to disassemble the supracapsules back into single nanocapsules, adding an external switch for the release of encapsulated cargoes. Such a disassembly ability could be especially useful for scenarios that require a single material with dynamically adjustable size, *e.g.* for delivering drug from arteries to arterioles and capillaries.[55–57]

In summary, the proposed microfluidic-assisted assembly strategy not only enables fine control over the formation of supracapsules, but also allows for a wide choice of building blocks. In the future, microfluidic assembly could be extended to nano-containers with various stimuli-responsive releases, endowing the resulting supracapsules with multiple release profiles, *e.g.* to fulfil the requirements for complex therapeutic delivery. We finally envision that this assembly strategy could have a significant impact not only in materials science, but also in other research fields such as biomedicine and artificial cells.

Materials and methods

Supracapsules synthesis

Supracapsules were prepared by the droplet-templated assembly of nanocapsules. Dextran-based nanocapsules were synthesized by a polyaddition reaction in a water-in-oil miniemulsion[44,45] (Fig. S1, ESI†). The resulting nanocapsule suspension was emulsified using a droplet-based microfluidic device containing a cross-junction (Fig. S2, ESI†) to form monodisperse oil droplets in a water phase containing 0.2 wt% of sodium dodecyl sulfate (SDS). The concentration of the nanocapsule suspension and the flow rates of oil phase and water phase in the microfluidic device were varied to control the final size of supracapsules. The generated oil-in-water emulsion was collected in an open Eppendorf tube to allow evaporation of cyclohexane inside a fume hood. After the evaporation, nanocapsules self-assembled to form supracapsules. The droplets and supracapsules were imaged by bright-field and fluorescence microscopy (using a Leica Eclipse inverted microscope). ImageJ was used to manually measure the sizes of over 100 droplets generated in the microfluidic device and the resulting supracapsules. Confocal microscopy was performed with a Nikon NSTORM (Nikon Ltd, UK) system equipped with a Rescan Confocal Microscope RCM1 (Confocal.nl, the Netherlands). We used a sCMOS camera (Orca Flash 4.0 V2) and a Nikon SR Apochromat TIRF 100× objective with oil immersion. The different laser excitations were at 488 nm and 647 nm, in order to excite the FITC and Cy5 dyes, respectively. The setup was fully controlled by NIS Elements (Nikon Ltd, UK). Multicolor z-stacks were acquired with a step size of 250 nm. Image analysis was performed using the open source FIJI ImageJ software and the NIS Elements from Nikon. The surface morphology of supracapsules was further characterized by SEM. The cross-section of supracapsules after cryo-cutting was imaged by cryo-SEM.

Magnetic response and guided motion of supracapsules

The magnetic properties of nanocapsules and supracapsules were measured by the vibrating sample magnetometry (PPMS Model 6000). Additionally, the magnetic supracapsules were placed in a Petri dish and their movement was controlled by displacing a permanent block magnet (NdFeB, Ø = 19.1 mm, height 6.4 mm) at different positions. The trajectories of supracapsules over time were analysed using ImageJ with particle Tracking MATLAB algorithms. To measure the oscillatory motion of supracapsules shown in Fig. S7 (ESI†), a customized setup with two pairs of independent Helmholtz coils[58] was used to generate an oscillatory magnetic field. The recorded image sequences were analysed using custom MATLAB algorithms to extract the positions of the supracapsules in each frame.

Release experiments

The release of the encapsulated payload in nanocapsules and supracapsules was measured using a fluorescence microplate reader (Spark 10M, TECAN) with λ_{ex} = 620 nm and λ_{em} = 680 nm. In order to monitor the payload release in an aqueous environment, nanocapsules in a cyclohexane suspension were redispersed into 0.2 wt% of SDS solution by solvent-exchange method (details in ESI†). The final concentration of Cy5 in nanocapsules suspension was diluted to 0.96 μmol L^{-1}. In order to compare the release profiles of nanocapsules and supracapsules with different sizes with the same total dye concentration, Cy5 concentration in the fabricated supracapsules was also adjusted to 0.96 μmol L^{-1} by adding the appropriate volume of 0.2 wt% of SDS solution. Subsequently, 50 μL aliquots of the aqueous suspensions at different periods of time were extracted and diluted with 450 μL of MilliQ water. The diluted sample was immediately centrifuged for 15 minutes using a relative centrifugal force of 14 000 to remove the nanocapsules or supracapsules. The supernatant was then collected and its fluorescence intensity was measured. The sediment was also collected at the end of the release experiment and redispersed in MilliQ water to measure the residual fluorescence intensity and estimate the amount of payload irreversibly attached to the nanocapsules or supracapsules after reaching the release equilibrium. The release experiments for each sample were repeated at least three times. Given that the total dye concentration is below the micromolar range, we can consider the solvent to act as a perfect sink at all times and thus apply the model reported in eqn (2).

Disassembly of supracapsules

1 mL of the prepared supracapsule suspension was first diluted into 9 mL of MilliQ water in a 15 mL glass vial. Sonication was applied by inserting a sonication tip (Fisher Scientific Q500 sonicator with a tip diameter of 6.2 mm) and sonicating with a cycle of 20 s pulse and 10 s pause at 20% amplitude. The

sonication times varied from 1 to 20 minutes. In the sonication-release experiment, a sonication time of 5 minutes was used. After sonication, the supracapsule cluster size was measured by dynamic light scattering (Zetasizer Nano ZS, Malvern).

All other methods and characterizations are described in details in ESI.†

Author contributions

Author contributions are defined based on the CRediT (Contributor Roles Taxonomy) and listed alphabetically. Conceptualization: M. H., L. I.; formal analysis: L. A., M. H., N. R.; funding acquisition: L. I.; investigation: L. A., M. H., N. R.; methodology: L. A., X. C., M. H., N. R., Y. X.; project administration: M. H., L. I.; resources: X. C., A. J. D., M. H., S. M., N. R., Y. X.; software: L. A.; supervision: M. H., L. I.; validation: M. H., N. R.; visualization: L. A., M. H., N. R., Y. X.; writing – original draft: M. H., L. I.; writing – review & editing: L. A., X. C., A. J. D., M. H., L. I., S. M., N. R., Y. X.

Conflicts of interest

There are no conflicts to declare.

Acknowledgements

The authors thank Stephan Handschin of ScopeM for the imaging of cryo-SEM and cryo-TEM, Dr Dorothea Pinotsi of ScopeM for the confocal imaging, Alexander Firlus for the VSM measurement and the help with analysis, Prof. Peter Fischer and Prof. Héloïse Thérien-Aubin for the insightful discussion of nanocapsules synthesis, and the Genetic Diversity Centre (GDC, ETH Zurich) for the support of fluorescence intensity measurement.

References

1 S. Wintzheimer, T. Granath, M. Oppmann, T. Kister, T. Thai, T. Kraus, N. Vogel and K. Mandel, Supraparticles: Functionality from uniform structural motifs, *ACS Nano*, 2018, **12**(6), 5093–5120.

2 S. Wooh, H. Huesmann, M. N. Tahir, M. Paven, K. Wichmann, D. Vollmer, W. Tremel, P. Papadopoulos and H. J. Butt, Synthesis of mesoporous supraparticles on superamphiphobic surfaces, *Adv. Mater.*, 2015, **27**(45), 7338–7343.

3 S. Li, J. Liu, N. S. Ramesar, H. Heinz, L. Xu, C. Xu and N. A. Kotov, Single-and multi-component chiral supraparticles as modular enantioselective catalysts, *Nat. Commun.*, 2019, **10**(1), 1–10.

4 D. Liu, R. Aleisa, Z. Cai, Y. Li and Y. Yin, Self-assembly of superstructures at all scales, *Matter*, 2021, **4**(3), 927–941.

5 K. Deng, Z. Luo, L. Tan and Z. Quan, Self-assembly of anisotropic nanoparticles into functional superstructures, *Chem. Soc. Rev.*, 2020, **49**(16), 6002–6038.

6 S. Wintzheimer, J. Reichstein, P. Groppe, A. Wolf, B. Fett, H. Zhou, R. Pujales-Paradela, F. Miller, S. Müssig and S. Wenderoth, Supraparticles for Sustainability, *Adv. Funct. Mater.*, 2021, **31**(11), 2011089.

7 Y. Xia, T. D. Nguyen, M. Yang, B. Lee, A. Santos, P. Podsiadlo, Z. Tang, S. C. Glotzer and N. A. Kotov, Self-assembly of self-limiting monodisperse supraparticles from polydisperse nanoparticles, *Nat. Nanotechnol.*, 2011, **6**(9), 580–587.

8 J. Wang, C. F. Mbah, T. Przybilla, B. A. Zubiri, E. Spiecker, M. Engel and N. Vogel, Magic number colloidal clusters as minimum free energy structures, *Nat. Commun.*, 2018, **9**(1), 1–10.

9 R. K. Shah, J. W. Kim and D. A. Weitz, Janus supraparticles by induced phase separation of nanoparticles in droplets, *Adv. Mater.*, 2009, **21**(19), 1949–1953.

10 T. Kister, M. Mravlak, T. Schilling and T. Kraus, Pressure-controlled formation of crystalline, Janus, and core–shell supraparticles, *Nanoscale*, 2016, **8**(27), 13377–13384.

11 Z. Yu, C. F. Wang, L. Ling, L. Chen and S. Chen, Triphase Microfluidic-Directed Self-Assembly: Anisotropic Colloidal Photonic Crystal Supraparticles and Multicolor Patterns Made Easy, *Angew. Chem.*, 2012, **124**(10), 2425–2428.

12 M. Xiao, J. Liu, Z. Chen, W. Liu, C. Zhang, Y. Yu, C. Li and L. He, Magnetic assembly and manipulation of Janus photonic crystal supraparticles from a colloidal mixture of spheres and ellipsoids, *J. Mater. Chem. C*, 2021, **9**, 11788–11793.

13 W. Liu, J. Midya, M. Kappl, H.-J. R. Butt and A. Nikoubashman, Segregation in drying binary colloidal droplets, *ACS Nano*, 2019, **13**(5), 4972–4979.

14 J. H. Bahng, S. Jahani, D. G. Montjoy, T. Yao, N. Kotov and A. Marandi, Mie resonance engineering in meta-shell supraparticles for nanoscale nonlinear optics, *ACS Nano*, 2020, **14**(12), 17203–17212.

15 Q. Fu, Y. Sheng, H. Tang, Z. Zhu, M. Ruan, W. Xu, Y. Zhu and Z. Tang, Growth mechanism deconvolution of self-limiting supraparticles based on microfluidic system, *ACS Nano*, 2015, **9**(1), 172–179.

16 W. Liu, M. Kappl and H.-J. R. Butt, Tuning the porosity of supraparticles, *ACS Nano*, 2019, **13**(12), 13949–13956.

17 H. Tan, S. Wooh, H.-J. Butt, X. Zhang and D. Lohse, Porous supraparticle assembly through self-lubricating evaporating colloidal ouzo drops, *Nat. Commun.*, 2019, **10**(1), 1–8.

18 B. Zhao, M. Borghei, T. Zou, L. Wang, L.-S. Johansson, J. Majoinen, M. H. Sipponen, M. Österberg, B. D. Mattos and O. J. Rojas, Lignin-Based Porous Supraparticles for Carbon Capture, *ACS Nano*, 2021, **15**(4), 6774–6786.

19 S. M. Jo, J. Kim, J. E. Lee, F. R. Wurm, K. Landfester and S. Wooh, Multimodal Enzyme-Carrying Suprastructures for Rapid and Sensitive Biocatalytic Cascade Reactions, *Adv. Sci.*, 2021, 2104884.

20 G. Jacucci, B. W. Longbottom, C. C. Parkins, S. A. Bon and S. Vignolini, Anisotropic silica colloids for light scattering, *J. Mater. Chem. C*, 2021, **9**(8), 2695–2700.

21 R. Savo, A. Morandi, J. S. Müller, F. Kaufmann, F. Timpu, M. R. Escalé, M. Zanini, L. Isa and R. Grange, Broadband Mie driven random quasi-phase-matching, *Nat. Photonics*, 2020, **14**(12), 740–747.

22 E. S. Goerlitzer, R. N. Klupp Taylor and N. Vogel, Bioinspired photonic pigments from colloidal self-assembly, *Adv. Mater.*, 2018, **30**(28), 1706654.
23 M. Hu, H.-J. r. Butt, K. Landfester, M. B. Bannwarth, S. Wooh and H. Thérien-Aubin, Shaping the assembly of superparamagnetic nanoparticles, *ACS Nano*, 2019, **13**(3), 3015–3022.
24 B. Bharti, A.-L. Fameau, M. Rubinstein and O. D. Velev, Nanocapillarity-mediated magnetic assembly of nanoparticles into ultraflexible filaments and reconfigurable networks, *Nat. Mater.*, 2015, **14**(11), 1104–1109.
25 A. Al Harraq, J. Lee and B. Bharti, Magnetic field–driven assembly and reconfiguration of multicomponent suprapartricles, *Sci. Adv.*, 2020, **6**(19), eaba5337.
26 U. Nayanathara, S. S. Kermaniyan and G. K. Such, Multicompartment Polymeric Nanocarriers for Biomedical Applications, *Macromol. Rapid Commun.*, 2020, **41**(18), 2000298.
27 L. Gautam, P. Shrivastava, B. Yadav, A. Jain, R. Sharma, S. Vyas and S. Vyas, Multicompartment systems: a putative carrier for combined drug delivery and targeting, *Drug Discovery Today*, 2021, **27**(4), 1184–1195.
28 N.-N. Deng, M. Yelleswarapu, L. Zheng and W. T. Huck, Microfluidic assembly of monodisperse vesosomes as artificial cell models, *J. Am. Chem. Soc.*, 2017, **139**(2), 587–590.
29 N.-N. Deng, M. Yelleswarapu and W. T. Huck, Monodisperse uni-and multicompartment liposomes, *J. Am. Chem. Soc.*, 2016, **138**(24), 7584–7591.
30 Y. Elani, R. V. Law and O. Ces, Vesicle-based artificial cells as chemical microreactors with spatially segregated reaction pathways, *Nat. Commun.*, 2014, **5**(1), 1–5.
31 R. J. Peters, M. Marguet, S. Marais, M. W. Fraaije, J. C. van Hest and S. Lecommandoux, Cascade reactions in multicompartmentalized polymersomes, *Angew. Chem.*, 2014, **126**(1), 150–154.
32 M. Marguet, L. Edembe and S. Lecommandoux, Polymersomes in polymersomes: multiple loading and permeability control, *Angew. Chem.*, 2012, **124**(5), 1199–1202.
33 S. Thamboo, A. Najer, A. Belluati, C. von Planta, D. Wu, I. Craciun, W. Meier and C. G. Palivan, Mimicking cellular signaling pathways within synthetic multicompartment vesicles with triggered enzyme activity and induced ion channel recruitment, *Adv. Funct. Mater.*, 2019, **29**(40), 1904267.
34 L. Zhang, K. Chen, H. Zhang, B. Pang, C. H. Choi, A. S. Mao, H. Liao, S. Utech, D. J. Mooney and H. Wang, Microfluidic templated multicompartment microgels for 3D encapsulation and pairing of single cells, *Small*, 2018, **14**(9), 1702955.
35 P. Majumder, U. Baxa, S. T. Walsh and J. P. Schneider, Design of a multicompartment hydrogel that facilitates time-resolved delivery of combination therapy and synergized killing of glioblastoma, *Angew. Chem., Int. Ed.*, 2018, **57**(46), 15040–15044.
36 L. Hosta-Rigau, M. J. York-Duran, Y. Zhang, K. N. Goldie and B. Städler, Confined multiple enzymatic (cascade) reactions within poly (dopamine)-based capsosomes, *ACS Appl. Mater. Interfaces*, 2014, **6**(15), 12771–12779.
37 M. Godoy-Gallardo, C. d. Labay, V. D. Trikalitis, P. J. Kempen, J. B. Larsen, T. L. Andresen and L. Hosta-Rigau, Multicompartment artificial organelles conducting enzymatic cascade reactions inside cells, *ACS Appl. Mater. Interfaces*, 2017, **9**(19), 15907–15921.
38 J. W. Maina, J. J. Richardson, R. Chandrawati, K. Kempe, M. P. Van Koeverden and F. Caruso, Capsosomes as long-term delivery vehicles for protein therapeutics, *Langmuir*, 2015, **31**(28), 7776–7781.
39 A. C. Misra and J. Lahann, Progress of Multicompartmental Particles for Medical Applications, *Adv. Healthcare Mater.*, 2018, **7**(9), 1701319.
40 M. Godoy-Gallardo, C. Labay, M. M. Jansman, P. K. Ek and L. Hosta-Rigau, Intracellular microreactors as artificial organelles to conduct multiple enzymatic reactions simultaneously, *Adv. Healthcare Mater.*, 2017, **6**(4), 1601190.
41 L. Wang, S. Song, J. van Hest, L. K. Abdelmohsen, X. Huang and S. Sánchez, Biomimicry of Cellular Motility and Communication Based on Synthetic Soft-Architectures, *Small*, 2020, **16**(27), 1907680.
42 S. Jiang, Caire da Silva, L. Ivanov, T. Mottola and M. Landfester, K., Synthetic Silica Nano-Organelles for Regulation of Cascade Reactions in Multi-Compartmentalized Systems, *Angew. Chem.*, 2021, e202113784.
43 Y. Yang, Y. Ning, C. Wang and Z. Tong, Capsule clusters fabricated by polymerization based on capsule-in-water-in-oil Pickering emulsions, *Polym. Chem.*, 2013, **4**(21), 5407–5415.
44 M. S. Alkanawati, M. Machtakova, K. Landfester and H. Thérien-Aubin, Bio-Orthogonal Nanogels for Multiresponsive Release, *Biomacromolecules*, 2021, **22**(7), 2976–2984.
45 M. S. Alkanawati, R. da Costa Marques, V. Mailänder, K. Landfester and H. Thérien-Aubin, Polysaccharide-Based pH-Responsive Nanocapsules Prepared with Bio-Orthogonal Chemistry and Their Use as Responsive Delivery Systems, *Biomacromolecules*, 2020, **21**(7), 2764–2771.
46 N. Vogel, S. Utech, G. T. England, T. Shirman, K. R. Phillips, N. Koay, I. B. Burgess, M. Kolle, D. A. Weitz and J. Aizenberg, Color from hierarchy: Diverse optical properties of micron-sized spherical colloidal assemblies, *Proc. Natl. Acad. Sci. U. S. A.*, 2015, **112**(35), 10845–10850.
47 M. Machtakova, S. Wirsching, S. Gehring, K. Landfester and H. Therien-Aubin, Controlling the semi-permeability of protein nanocapsules influences the cellular response to macromolecular payloads, *J. Mater. Chem. B*, 2021, **9**, 8389–8398.
48 P. Costa and J. M. S. Lobo, Modeling and comparison of dissolution profiles, *Eur. J. Pharm. Sci.*, 2001, **13**(2), 123–133.
49 S. Muschert, F. Siepmann, B. Leclercq, B. Carlin and J. Siepmann, Prediction of drug release from ethylcellulose coated pellets, *J. Controlled Release*, 2009, **135**(1), 71–79.
50 M. S. Birajdar and J. Lee, Sonication-triggered zero-order release by uncorking core–shell nanofibers, *Chem. Eng. J.*, 2016, **288**, 1–8.
51 A. L. White, C. Langton, M.-L. Wille, J. Hitchcock, O. J. Cayre, S. Biggs, I. Blakey, A. K. Whittaker, S. Rose and S. Puttick, Ultrasound-triggered release from metal shell microcapsules, *J. Colloid Interface Sci.*, 2019, **554**, 444–452.

52 J. Zhang, Y. Zheng, J. Lee, J. Hua, S. Li, A. Panchamukhi, J. Yue, X. Gou, Z. Xia and L. Zhu, A pulsatile release platform based on photo-induced imine-crosslinking hydrogel promotes scarless wound healing, *Nat. Commun.*, 2021, **12**(1), 1–13.

53 Y. Ma, C. Cortez-Jugo, J. Li, Z. Lin, R. T. Richardson, Y. Han, J. Zhou, M. Björnmalm, O. M. Feeney and Q.-Z. Zhong, Engineering biocoatings to prolong drug release from supraparticles, *Biomacromolecules*, 2019, **20**(9), 3425–3434.

54 D. Maiolo, C. Pigliacelli, P. Sánchez Moreno, M. B. Violatto, L. Talamini, I. Tirotta, R. Piccirillo, M. Zucchetti, L. Morosi and R. Frapolli, Bioreducible hydrophobin-stabilized supraparticles for selective intracellular release, *ACS Nano*, 2017, **11**(9), 9413–9423.

55 J. Zhang, Z. Di, H. Yan, Y. Zhao and L. Li, One-Step Synthesis of Single-Stranded DNA-Bridged Iron Oxide Supraparticles as MRI Contrast Agents, *Nano Lett.*, 2021, **21**(7), 2793–2799.

56 M. Ma, H. Zhu, J. Ling, S. Gong, Y. Zhang, Y. Xia and Z. Tang, Quasi-amorphous and Hierarchical Fe_2O_3 Supraparticles: Active T 1-Weighted Magnetic Resonance Imaging *in Vivo* and Renal Clearance, *ACS Nano*, 2020, **14**(4), 4036–4044.

57 Q. Wang, K. F. Chan, K. Schweizer, X. Du, D. Jin, S. C. H. Yu, B. J. Nelson and L. Zhang, Ultrasound Doppler-guided real-time navigation of a magnetic microswarm for active endovascular delivery, *Sci. Adv.*, 2021, **7**(9), eabe5914.

58 I. Buttinoni, Z. A. Zell, T. M. Squires and L. Isa, Colloidal binary mixtures at fluid–fluid interfaces under steady shear: structural, dynamical and mechanical response, *Soft Matter*, 2015, **11**(42), 8313–8321.

